ELSEVIER

Journal of Alloys and Compounds 446–447 (2007) 96–100

Journal of ALLOYS AND COMPOUNDS

www.elsevier.com/locate/jallcom

Energy density analysis of the chemical bond between atoms in perovskite-type hydrides

Yoshifumi Shinzato [a,*], Hiroshi Yukawa [a], Masahiko Morinaga [a], Takeshi Baba [b], Hiromi Nakai [b]

[a] *Department of Materials Science and Engineering, Graduate School of Engineering, Nagoya University, Furo-cho, Chikusa-ku, Nagoya 464-8603, Japan*

[b] *Department of Chemistry, School of Science and Engineering, Waseda University, Okubo, Shinjuku-ku, Tokyo 169-8555, Japan*

Received 28 September 2006; received in revised form 16 January 2007; accepted 19 February 2007
Available online 25 February 2007

Abstract

Atomization energy diagram is proposed for analyzing the chemical bond in the perovskite-type hydrides such as $M1MgH_3$ (M1 = Na, K, Rb), $RbCaH_3$, $CaNiH_3$ and $SrPdH_3$. The atomization energies of hydrogen and metal atoms in the hydrides are evaluated theoretically by the energy density analysis (EDA) of the total energy, and used for the construction of the atomization energy diagram. Every hydride can be located in such an energy diagram, although there are differences in the nature of the chemical bond among the hydrides. When the hydrides have a resemblance in the chemical bond, their locations are close to each other in the diagram. The role of constituent elements in the hydride is understood well with the aid of this diagram. For comparison, the atomization energy diagram is shown for the perovskite-type oxides.

Keywords: Perovskite-type hydrides; Energy density analysis; Chemical bond; Atomization energy; Perovskite-type oxides

1. Introduction

In 1955 Wigner and Seitz [1] predicted that if one had a great calculating machine, one might apply it to the problem of solving the Schrödinger equation for each metal and obtain the interesting physical quantities, such as the cohesive energy, the lattice constant and similar parameter. It is not clear, however, that a great deal would be gained by this. Presumably the results would agree with the experimentally determined quantities and nothing vastly new would be learned from the calculation. This prediction made by two pioneers of solid state physics remains true in these days, even though the computational science has made great progress.

In addition, the Mulliken population analysis [2] is so common in the field of molecular orbital calculations, and the nature of the chemical bond between atoms has been treated well by using a standard concept of covalent or ionic bond. However, with this analysis, it is still difficult to compare quantitatively the chemical bond strength among a variety of materials. To solve this problem, the chemical bond should be estimated quantitatively in an energy scale.

Recently, Nakai has proposed a new analyzing technique called energy density analysis (EDA) [3]. In this method, the total energy of a system, computed by using the Kohn–Sham type density functional theory (DFT) [4], is partitioned into atomic energy densities, and the characteristics of the chemical bond are understood in terms of each atomic energy density instead of using the total energy. In this paper, the atomization energy of the respective atom in the perovskite-type hydrides (e.g., $M1MgH_3$ (M1 = Na,K,Rb)), is obtained by subtracting the atomic energy density from the energy of an isolated atomic state. Then, an atomization energy diagram is proposed for the first time in order to understand the nature of the chemical bond in an energy scale. For comparison, the approach is further extended to the perovskite-type oxides such as $CaM2O_3$ and $SrM2O_3$ (M2 = Ti, Zr).

* Corresponding author.
E-mail address: shinzato@silky.numse.nagoya-u.ac.jp (Y. Shinzato).

0925-8388/$ – see front matter © 2007 Elsevier B.V. All rights reserved.
doi:10.1016/j.jallcom.2007.02.116

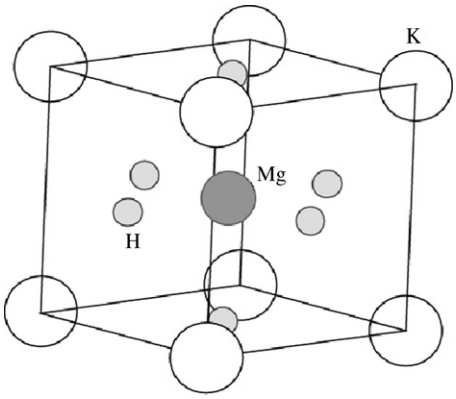

Fig. 1. Crystal structure of perovskite-type hydride, $KMgH_3$.

2. Calculation procedure

2.1. Geometry optimization

The crystal structure of perovskite-type hydride, $KMgH_3$, is illustrated in Fig. 1. This is a cubic structure in which potassium, magnesium and hydrogen occupy a corner, a center and a face-center of the cube, respectively. Some hydrides have non-cubic structure due to the distortion, and form, for example, hexagonal or orthorhombic structure. The positions of hydrogen in hydrides are sometimes difficult to be determined experimentally. So, in this study, the crystal structures of perovskite-type hydrides are optimized by the total energy minimization using the plane-wave pseudopotentital method.

For this purpose, the first-principle calculations based on the density functional theory are performed with a generalized gradient approximation (GGA) by Perdew et al [5]. The implementation of DFT employed here combines a plane-wave basis set with the total energy pseudopotential method, as is embodied in the CASTEP code [6]. The present calculations used are based upon the ultrasoft pseudopotentials proposed by Vanderbilt [7]. The plane-wave cutoff energy is chosen to be 380 eV, because this cutoff energy is found to achieve the convergence of the total energies within 0.03 eV, as compared to the results with the cutoff energies up to 600 eV. The sampling in the reciprocal space is done with the k-points grids of $6 \times 6 \times 6$ for orthorhombic $NaMgH_3$ [8], $6 \times 6 \times 6$ for cubic $KMgH_3$ [9], $5 \times 5 \times 2$ for hexagonal $RbMgH_3$ [10], $6 \times 6 \times 4$ for cubic $RbCaH_3$ [11], $8 \times 8 \times 8$ for cubic $CaNiH_3$ [12], $8 \times 8 \times 8$ for cubic $SrPdH_3$ [13]. The calculated lattice parameters agree with the measured ones [8–13] within 1.2%. The further explanation of the calculation method is given elsewhere [14,15].

2.2. Energy density analysis (EDA)

The electronic structures for optimized crystal lattice of hydrides are obtained by the DFT calculations under the periodic boundary condition (PBC) using Gaussian03 program package. The adopted functional is the BLYP functional, which consist of the Slater exchange [16], the Becke (B88) exchange [17], the Vosco–Wilk–Nusair (VWN) correlation [18] and the Lee–Yang–Parr (LYP) correlation functionals [19]. The following modified Gaussian basis sets are adopted: the correlation-consistent polarization plus the valence double zeta (cc-pVDZ) basis sets of Dunning [20,21] without d-type functions for H, Li, Na and Mg, the Arlrichs TZV basis set [22] without the outer s function for K, the Huginaga basis set [23] without the outer s function and constructed to be double zeta class for Rb. The EDA calculations under PBC [24] are performed by linking the original code for the EDA with Gaussian03 [25].

Following the EDA, the atomic energy density of A atom is evaluated by,

$$E^{\mathrm{A}} = E^{\mathrm{A}}_{\mathrm{NN}} + T^{\mathrm{A}}_{\mathrm{S}} + E^{\mathrm{A}}_{\mathrm{Ne}} + E^{\mathrm{A}}_{\mathrm{CLB}} + E^{\mathrm{A}}_{\mathrm{XC}}. \quad (1)$$

where $E^{\mathrm{A}}_{\mathrm{NN}}$ is the nuclear–nuclear repulsion energy density, $T^{\mathrm{A}}_{\mathrm{S}}$ is the non-interacting kinetic energy density, $E^{\mathrm{A}}_{\mathrm{Ne}}$ is the nuclear–electron attraction energy density, $E^{\mathrm{A}}_{\mathrm{CLB}}$ is the Coulomb energy density, $E^{\mathrm{A}}_{\mathrm{XC}}$ is the exchange-correlation energy density.

In Eq. (1), for example, $E^{\mathrm{A}}_{\mathrm{XC}}$ is evaluated by the partial sum for the numerical quadrature technique,

$$E^{\mathrm{A}}_{\mathrm{XC}} = \sum_{\mathrm{g}}^{\mathrm{grid}} \omega_{\mathrm{g}} p_{\mathrm{A}}(r_{\mathrm{g}}) F_{\mathrm{XC}}(r_{\mathrm{g}}), \quad (2)$$

where $\omega_{\mathrm{g}}(r_{\mathrm{g}})$ is the weighting factor, $p_{\mathrm{A}}(r_{\mathrm{g}})$ is the partition function, and $F_{\mathrm{XC}}(r_{\mathrm{g}})$ is the exchange-correlation functional. The other terms in Eq. (1), which are evaluated by the analytical integration with the Kohn–Sham orbitals, are partitioned into their energy densities on the analogy of Mulliken population analysis [2].

2.3. Atomization energy

The EDA analysis is performed with the geometry optimized by the plane-wave pseudopotential method. For binary hydrides, MH, the respective atomic energy densities of M and H are related closely to the nature of the chemical bond relevant to M and H atoms in MH. When the energy of the isolated neutral atom, $E^{\mathrm{atom}}_{\mathrm{M}}$ (or $E^{\mathrm{atom}}_{\mathrm{H}}$), is taken as a reference, the atomization energy, ΔE_{M} (or ΔE_{M}) is defined as,

$$\Delta E_{\mathrm{M}} = E^{\mathrm{atom}}_{\mathrm{M}} - E^{\mathrm{hydride}}_{\mathrm{M}}, \quad (3)$$

$$\Delta E_{\mathrm{H}} = E^{\mathrm{atom}}_{\mathrm{H}} - E^{\mathrm{hydride}}_{\mathrm{H}}, \quad (4)$$

where $E^{\mathrm{hydride}}_{\mathrm{M}}$ and $E^{\mathrm{hydride}}_{\mathrm{H}}$ are the atomic energy densities for M and H in MH, respectively. In case of the perovskite-type hydrides, $M1M2H_3$, ΔE_{M} is defined as $(\Delta E_{\mathrm{M1}} + \Delta E_{\mathrm{M2}})/3$, that is the average atomization energy of M1 and M2 to be counted per hydrogen atom. The cohesive energy, E_{coh}, of the hydride per hydrogen atom is defined as,

$$\Delta E_{\mathrm{M}} + \Delta E_{\mathrm{H}} = E_{\mathrm{coh}} \quad (5)$$

Here, the energy of the isolated atom is used as a reference following the definition of E_{coh} given by Kittel [26]. Thus, ΔE_{M} and ΔE_{H} are the components of E_{coh}. So, each of atomization energy energies become a measure of the chemical bonding effect of the

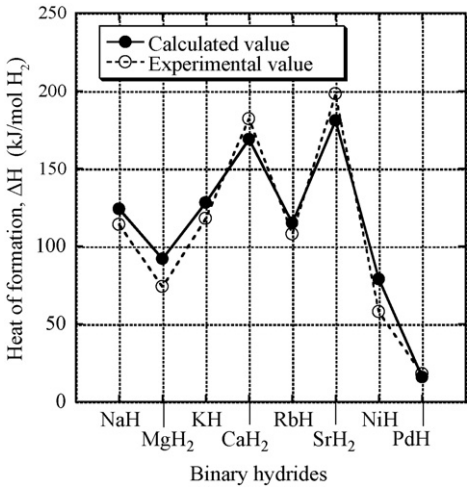

Fig. 2. Calculated and experimental heat of formation for binary hydrides.

element on the stability of the hydrides. By setting that $y = \Delta E_H$ and $x = \Delta E_M$, we obtain a relation, $y = -x + E_{coh}$. So, E_{coh} is expressed as a point of intersection between this line and y-axis at $x = 0$.

3. Results and discussion

3.1. Heat of formation and cohesive energy for binary hydrides

First, to show the reliability of the present calculation, the heat of formation, ΔH, for binary hydrides, MH_n, is calculated assuming that $M + (n/2)H_2 \rightarrow MH_n$ and compared with the experiment [27]. As shown in Fig. 2, there is good agreement between the calculated and the experimental values.

The cohesive energy, E_{coh}, is a measure of the electronic stability of hydrides. As shown Table 1, the difference between the calculated and the experimental values for E_{coh} lies within 0.44 eV [28]. Thus, the present calculation is performed in a reasonable manner.

3.2. Atomization energy diagram

The calculated atomization energies are listed in Table 2. In every perovskite-type hydride, the value of ΔE_H is larger than ΔE_{M1} and ΔE_{M2}, indicating that hydrogen contributes significantly to the electronic stability of these hydrides.

Table 1
Calculated and measured cohesive energy for binary hydrides (eV)

	E_{coh} (Calculated)	E_{coh} (Experimental)
NaH	4.39	3.96
MgH_2	3.34	3.41
KH	3.38	3.78
CaH_2	4.27	4.12
RbH	3.34	3.64
SrH_2	3.76	4.04
NiH	7.20	7.32
PdH	6.17	6.58

Table 2
Calculated atomization energy for binary hydrides and perovskite-type hydrides (eV)

	ΔE_M	ΔE_H		ΔE_{M1}	ΔE_{M2}	ΔE_M	ΔE_H
NaH	4.58	−0.19	NaMgHs	1.38	1.64	1.01	2.72
MgH_2	0.76	2.96	KMgHs	−0.74	−1.27	−0.67	4.10
KH	−1.11	4.49	RbMgHs	−0.22	0.40	0.06	3.34
CaH_2	−1.45	4.99	RbCaHs	−1.10	−1.03	−0.71	4.79
RbH	−5.11	8.45	CaNiHs	−5.89	−4.83	−3.57	8.80
SrH_2	−4.05	5.79	SrPdHs	−3.47	−14.47	−5.98	10.33
NiH	−4.44	11.64					
PdH	−10.29	16.46					

For perovskite-type hydrides and their constituent metal-based binary hydrides, a ΔE_H versus ΔE_M diagram is constructed in an energy scale as shown in Fig. 3. This ΔE_H versus ΔE_M diagram is hereafter called "atomization energy diagram". By using this atomization energy diagram, every hydride can be shown in one figure, although there are significant differences in the nature of the chemical bond among them.

As a whole, there is a clear trend that ΔE_H increases with decreasing ΔE_M. ΔE_H is positive, but ΔE_M is negative in most cases. Thus, the hydrogen state is more stabilized in the hydride than in the isolated atomic state, while the M state is destabilized in most hydrides. In other words, the stabilized H state emerges in compensation for the destabilized M state in most hydrides. From this view point, NaH is a unique hydride where the Na state is stabilized rather than the H state. An ionic crystal, NaCl has the same trend as NaH.

3.2.1. Binary hydrides

Needless to say, when the hydrides have a resemblance in the chemical bonding state, their locations are close to each other in the diagram. For example, binary hydrides of transition elements (i.e., NiH and PdH) appear in the higher ΔE_H region than those of typical elements (i.e., NaH, MgH_2, KH, CaH_2, SrH_2 and RbH). Thus, transition elements could stabilize the hydrogen state remarkably in the binary hydrides probably owing to

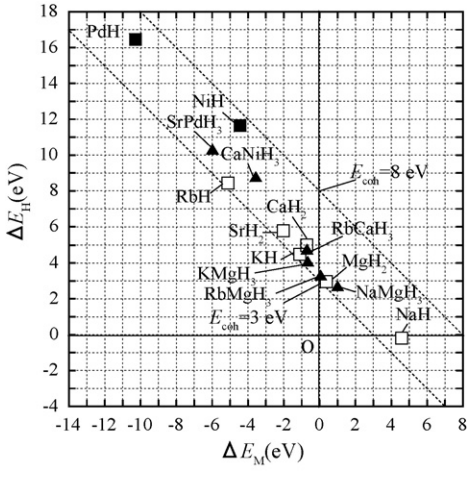

Fig. 3. Atomization energy diagram for perovskite-type hydrides and binary hydrides.

the covalent interaction operating between hydrogen and transition elements. On the other hand, binary hydrides of typical elements have a lower ΔE_H, probably owing to the ionic interaction mainly operating between hydrogen and typical elements in them. As a result, binary hydrides of transition elements have larger cohesive energy, E_{coh}, than those of typical elements, as listed in Table 1.

Among binary alkali metal hydrides with the same crystal structure, the atomization energy for hydrogen, ΔE_H, changes in the order, NaH < KH < RbH. According to the Mulliken population analysis [2], the net charges on the hydrogen atom in them change in the order, NaH (−0.55) > KH (−0.71) ≈ RbH (−0.71). This means that charge transfer occurs from metal to hydrogen atoms in them. The amount of transferred charges is larger in KH and RbH than in NaH, in agreement with the electronegativity of each metal atom. Thus, the hydrogen state in these hydrides is stabilized to some extent by the charge transfer. However, such a traditional analysis never explains a whole feature of the atomization energy diagram expressed in an energy scale.

3.2.2. *Perovskite-type hydrides*

For any perovskite-type hydrides, $M1M2H_3$, it is known that the M1–H and M2–H interactions are rather ionic in character, even though covalent character still remains to some extent in the M2–H bond because of the shorter M2–H distance than the M1–H one. This is the case of the perovskite-type hydrides of typical elements (e.g., $NaMgH_3$, $RbCaH_3$). On the other hand, the covalent character further increases in case when M2 is a transition element. This is the case of the perovskite-type hydrides of transition elements (e.g., $CaNiH_3$ and $SrPdH_3$). As a result, $CaNiH_3$ and $SrPdH_3$ possess a larger ΔE_H than $NaMgH_3$ and $RbCaH_3$ as shown in Fig. 3.

In addition, this diagram enables us to understand the chemical reaction for the formation of pervoskite-type hydrides. For example, for a chemical reaction, $NaH + MgH_2 \rightarrow NaMgH_3$, it is found that $NaMgH_3$ is located just in between NaH and MgH_2 in this diagram. This indicates that $NaMgH_3$ inherits the nature of the chemical bond from NaH and MgH_2 to some extent. This trend is seen in the other perovskite-type hydrides as shown in Fig. 3.

Among the Mg-based perovskite-type hydrides, $M1MgH_3$ (M1 = Na, K, Rb), $NaMgH_3$ and $RbMgH_3$ are located near MgH_2 rather than NaH or RbH. The chemical bond in $NaMgH_3$ and $RbMgH_3$ has a resemblance to the chemical bond in MgH_2 to some extent. On the other hand, $KMgH_3$ is located near KH rather than MgH_2. So, there is a resemblance in the chemical bond between $KMgH_3$ and KH. However, fine adjustment to the chemical bond still takes place in these hydrides, as explained in Section 3.3.

3.3. ΔE_{M1} versus ΔE_{M2} diagram

A ΔE_{M1} versus ΔE_{M2} diagram is also constructed on the basis of the present calculation to understand the role of metal elements in the formation of the chemical bond in the hydride. The results are shown in Fig. 4. ΔE_{M1} (or ΔE_{M2}) is a measure of the M1 (or M2) contribution to the cohesive energy of the perovskite-type hydride. A line showing a relation, $\Delta E_{M1} = \Delta E_{M2}$, is drawn in Fig. 4. All the pervoskite-type hydrides except for $SrPdH_3$ are located along this line. This implies that the M1 and M2 metallic states are well balanced in the perovskite-type hydrides, and their contribution to the cohesive energy is nearly equal. However, such a balance is no longer present in $SrPdH_3$ containing Pd, where the strong covalent interaction between Pd and H atoms breaks the balance, resulting in a large, negative ΔE_{Pd} and in a large, positive ΔE_H, while showing a small, negative ΔE_{Sr}.

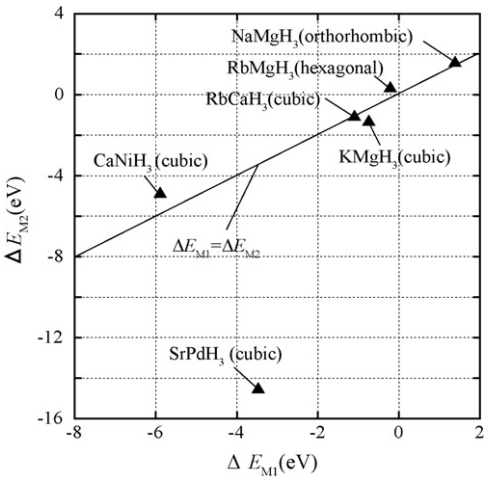

Fig. 4. ΔE_{M1} vs. ΔE_{M2} diagram for perovskite-type hydrides.

3.4. *Comparison between perovskite-type hydrides and oxides*

The atomization energy diagram is shown in Fig. 5 for the perovskite-type oxides, $M1M2O_3$, where M2 are the transition elements such as Ti and Zr. As a whole, there is a trend that ΔE_M and ΔE_O are both positive in most cases. This is in contrast with the trend of negative ΔE_M and positive ΔE_H observed in the

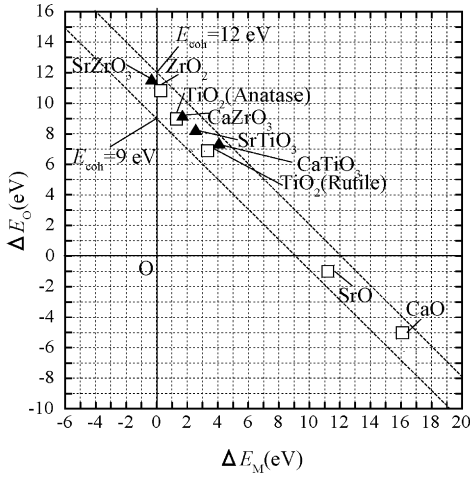

Fig. 5. Atomization energy diagram for perovskite-type oxides and binary oxides.

perovskite-type hydrides as shown in Fig. 3. In addition, there is a trend that ΔE_O decreases with increasing ΔE_M. As a result, E_{coh} lies in the range of 9–12 eV, which is larger than the value for hydrides listed in Table 2. Also, most of the binary oxides containing transition elements appear in the higher ΔE_O region than the oxides containing typical elements, which is also found in the perovskite-type hydrides as explained earlier. In addition, it is stressed here that the perovskite-type oxides, $M1M2O_3$, are located near the binary oxides, $M2O_n$, in the diagram, indicating that the perovskite-type oxide, $M1M2O_3$ inherits the nature of the chemical bond mainly from $M2O_n$.

In Fig. 5, all the oxides follow a simple trend $\Delta E_O = -\Delta E_M + E_{coh}$ (= nearly constant). This is attributable to the smaller change in the E_{coh} value among the oxides, as compared to the relatively larger change in both ΔE_O and ΔE_M. In other words, the electronic states of M and O atoms are adjusted largely depending on M, so as to keep an E_{coh} value nearly constant. Thus, a beautiful energy balance lying between the M and O atoms probably causes a simple trend in the oxides. Such a trend is also seen in the hydrides as shown in Fig. 3.

However, when constituent elements is fixed, this is not the case. One extreme example is seen in organic liquid systems, benzene (C_6H_6), cyclohexane (C_6H_{12}), naphthalene ($C_{10}H_8$) and decalin ($C_{10}H_{18}$). These are important organic systems for hydrogen storage. In these four systems, every ΔE_H value is nearly same and only the ΔE_C values vary largely depending on the molecules. So, the sum of them defined as E_{coh} changes significantly with the molecules, and hence a simple trend is no longer satisfied in them.

4. Conclusion

A unified approach based on the atomization energy concept is proposed for understanding the chemical bond in perovskite-type hydrides and oxides without using a standard concept of covalent bond or ionic bond.

An atomization energy diagram is constructed for the first time to treat the chemical interactions in the perovskite-type hydrides and oxides in an energy scale. The diagram reflects well characteristics of the chemical bond, for example, the atomization energy of hydrogen (or oxygen) changes largely with the covalent or ionic interactions. Also, since the sum of the atomization energy equals the cohesive energy, each of atomization energies becomes a measure of the chemical bonding effect of the element on the stability of the hydride (or oxide). The atomization energy is balanced well among the constituent elements. For example, for the perovskite-type hydrides, $M1M2H_3$, being composed of typical elements, M1 and M2, fine adjustment to the chemical bond makes a nice balance in the atomization energy between M1 and M2, i.e., $\Delta E_{M1} \approx \Delta E_{M2}$.

Acknowledgments

The authors would like to express sincere thanks to the staff of the Computer Center, Institute for Molecular Science, Okazaki National Institute for the use of super-computers. This study was supported by a Grant-in-Aid for Scientific Research from the Ministry of Education, Culture, Sports, Science and Technology of Japan, and by the Japan Society for the Promotion of Science, and also by the 21st Century COE program "Nature-Guided Materials Processing" of the Ministry of Education, Culture, Sports, Science and Technology.

References

[1] E.P. Wigner, F. Seitz, Solid State Phys. 1 (1955) 97–126.
[2] R.S. Mulliken, J. Chem. Phys. 23 (1955) 1833–1840.
[3] H. Nakai, Chem. Phys. Lett. 363 (2002) 73–79.
[4] W. Kohn, L.J. Sham, Phys. Rev. 140 (1965) A1133–A1138.
[5] J.P. Perdew, K. Burke, Y. Wang, Phys. Rev. B 41 (1970) 7892–7895.
[6] V. Milman, B. Winkler, J.A. White, C.J. Pickard, M.C. Payne, E.V. Akhmatsukaya, R.H. Nodes, Int. J. Quantum Chem. 77 (2000) 895–910.
[7] D. Vanderbilt, Phys. Rev. B 41 (1990) 7892–7895.
[8] A. Bouamrane, J.P. Laval, J.P. Soulie, J.P. Bastide, Mater. Res. Bull. 35 (2000) 545–549.
[9] J.P. Bastide, A. Bouamrane, P. Caludy, J.M. Letoffe, J. Less-Common Met. 136 (1987) L1–L4.
[10] F. Gingl, T. Vogt, E. Akiba, K. Yvon, J. Alloys Compd. 282 (1999) 125–129.
[11] H.H. Park, M. Pezat, B. Darriet, C. R. Acad. Sci. Ser. 2 306 (1988) 963–965.
[12] T. Sato, D. Noreus, H. Takeshita, U. Haussermann, J. Solid State Chem. 178 (2005) 3381–3388.
[13] W. Bronger, G. Ridder, J. Alloys Compd. 210 (1994) 53–55.
[14] M. Yoshino, K. Komiya, Y. Takahashi, Y. Shinzato, H. Yukawa, M. Morinaga, J. Alloy. Compd. 404–406 (2005) 185–190.
[15] M. Yoshino, Y. Shinzato, M. Morinaga, Mater. Sci. Forum 449–452 (2004) 287–290.
[16] J.C. Slater, Phys. Rev. 81 (1951) 385–390.
[17] A.D. Becke, Phys. Rev. A. 38 (1988) 3098–3100.
[18] S.H. Vosco, L. Wilk, M. Nusair, Can. J. Phys. 58 (1980) 1200–1211.
[19] C. Lee, W. Yang, R.G. Parr, Phys. Rev. B. 37 (1988) 785–789.
[20] T.H. Dunning Jr., J. Chem. Phys. 90 (1989) 1007–1023.
[21] D.E. Woon, T.H. Dunning Jr., J. Chem. Phys. 98 (1993) 1358–1371.
[22] A. Schafer, C. Huber, R. Ahlrichs, J. Chem. Phys. 100 (1994) 5829–5835.
[23] S. Huzinaga, J. Andzelm, M. Klobukowski, E. Radzioandzelm, Y. Sakai, H. Tatewaki, Gaussian Basis Sets for Molecular Calculation, Elsevier, New York, 1984.
[24] H. Nakai, Y. Kurabayashi, M. Katouda, T. Atsumi, Chem. Phys. Lett., in press.
[25] M.J. Frisch, G.W. Trucks, H.B. Schlegel, G.E. Scuseria, M.A. Robb, J.R. Cheeseman, J.A. Montgomery Jr., T. Vreven, K.N. Kudin, J.C. Burant, J.M. Millam, S.S. Iyengar, J. Tomasi, V. Barone, B. Mennucci, M. Cossi, G. Scalmani, N. Rega, G.A. Petersson, H. Nakatsuji, M. Hada, M. Ehara, K. Toyota, R. Fukuda, J. Hasegawa, M. Ishida, T. Nakajima, Y. Honda, O. Kitao, H. Nakai, M. Klene, X. Li, J.E. Knox, H.P. Hratchian, J.B. Cross, V. Bakken, C. Adamo, J. Jaramillo, R. Gomperts, R.E. Stratmann, O. Yazyev, A.J. Austin, R. Cammi, C. Pomelli, J.W. Ochterski, P.Y. Ayala, K. Morokuma, G.A. Voth, P. Salvador, J.J. Dannenberg, V.G. Zakrzewski, S. Dapprich, A.D. Daniels, M.C. Strain, O. Farkas, D.K. Malick, A.D. Rabuck, K. Raghavachari, J.B. Foresman, J.V. Ortiz, Q. Cui, A.G. Baboul, S. Clifford, J. Cioslowski, B.B. Stefanov, G. Liu, A. Liashenko, P. Piskorz, I. Komaromi, R.L. Martin, D.J. Fox, T. Keith, M.A. Al-Laham, C.Y. Peng, A. Nanayakkara, M. Challacombe, P.M.W. Gill, B. Johnson, W. Chen, M.W. Wong, C. Gonzalez, J.A. Pople, Gaussian Inc., Wallingford, CT, 2004.
[26] C. Kittel, Introduction to Solid State Physics, Wiley, 1986.
[27] Y. Fukai, The Metal–Hydrogen System, Springer-Verlag, 1994.
[28] R.C. Weast, M.J. Astle, W.H. Beyer, CRC Handbook of Chemistry and Physics: A Ready-Reference Book of Chemical and Physical Data, 84th ed., CRC Press, 2003.